

Integrating geometric and biomechanical models of a liver tumour for cryosurgery simulation

Alexandra Branzan Albu¹, Jean-Marc Schwartz¹, Denis Laurendeau¹, and Christian Moisan²

¹ Computer Vision and Systems Laboratory, Department of Electrical and Computer Engineering, Laval University, Québec (Qc) G1K 7P4, Canada
{Branzan, Schwartz, Laurend}@gel.ulaval.ca

² IMRI Unit, Québec City University Hospital, Québec (Qc) G1L 3L5, Canada
{Christian.Moisan}@rad.ulaval.ca

Abstract. In this paper, we present a 3D reconstruction approach of a liver tumour model from a sequence of 2D MR parallel cross-sections, and the integration of this reconstructed 3D model with a mechanical tissue model. The reconstruction algorithm uses shape-based interpolation and extrapolation. While interpolation generates intermediate slices between every pair of adjacent input slices, extrapolation performs a smooth closing of the external surface of the model. Interpolation uses morphological morphing, while extrapolation is based on smoothness surface constraints. Local surface irregularities are further smoothed with Taubin's surface fairing algorithm [5]. Since tumour models are to be used in a planning and simulation system of image-guided cryosurgery, a mechanical model based on a non-linear tensor-mass algorithm was integrated with the tumour geometry. Integration allows the computation of fast deformations and force feedback in the process of cryoprobe insertion.

1 Introduction

Widely used medical imaging systems based on MR, X-rays, positron-emission, or ultrasound scan 3D anatomic structures in a sequence of 2D parallel image slices. In order to visualize, analyze and manipulate this data, one has to deal with the difference between the inter- and intra-slice resolution. Usually, the intra-slice resolution is much higher than the inter-slice resolution, due to technical limitations and/or medical reasons (respiratory motion artefact, limited interval of exposure etc.). This is why interpolation and/or extrapolation techniques are required to estimate the missing slices. While a great variety of interpolation methods are available in the medical imaging literature, extrapolation techniques are rare, probably because of the difficulty in validating the results.

Grey-level interpolation techniques [1][2] consist of direct computation of intensity for every pixel in the interpolated slice. Since medical imaging applications are strongly object-oriented, the main drawback of grey-level interpolation techniques consists in the large amount of input data for further segmentation, and errors occurring in segmentation due to prior interpolation. Shape-based interpolation techniques

are object-oriented and interpolate the binary object cross-section rather than the grey-scale intensity values. A general object reconstruction method based on deformable meshes is proposed in [3]. There is also a rich literature in spline-based interpolation techniques [4]. Mathematical morphology offers a coherent framework for developing effective shape-based interpolation algorithms. The morphological morphing transform in [5] interpolates a new group of slices between each two consecutive input slices, by performing a gradual shape transition. Our proposed scheme is similar to this approach. However, their morphing approach is based on iterative erosion and we observed that, in the case of a non-convex initial shape, iterative erosion may divide the foreground into disjoint regions, thus hindering a smooth shape transition. Instead, we propose a morphing technique based on conditional dilation. Furthermore, we are able to obtain a uniform inter-slice resolution by adjusting the lengths of the morphing sequences.

In this paper, we propose a 3D reconstruction approach using shape-based interpolation and extrapolation. To obtain maximum overlapping between adjacent slices, a *shape alignment* step is necessary prior to morphing. The interpolation process is based on *morphing*, thus performing a smooth transition between every two adjacent input slices. Next, a *closing surface* step is performed using an extrapolation technique. The 3D reconstructed model integrates the “closing” and “morphing” sequences in a coherent manner, featuring an adjustable uniform inter-slice resolution. Figure 1 presents the diagram of the proposed reconstruction process.

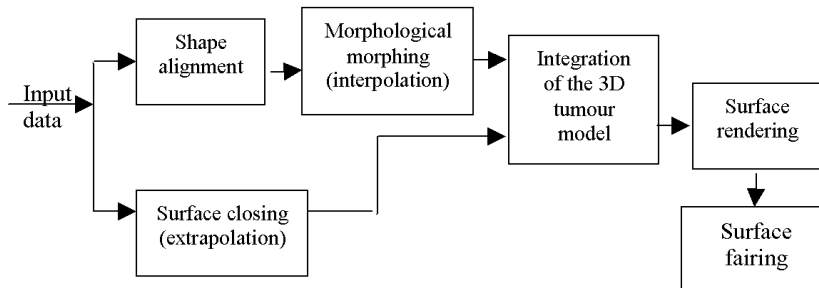


Figure 1. The diagram of the proposed reconstruction process

The organization of this paper is as follows. Section 2 presents the proposed 3D reconstruction approach. Section 3 shows and validates our reconstruction results, while section 4 describes the integration of the geometric model with a mechanical tissue model. Finally, we draw the conclusions and describe future work.

2 Reconstruction approach

For every patient, a serial sequence of 2D MR segmented images of transversal liver slices is provided. The foreground of each segmented image represents a cross-section through the targeted tumour. The used segmentation method has been described in [6]. Respiratory movements prevent the slice thickness from being reduced below 10 mm

in the abdominal MR image acquisition process. Small liver tumours of 5 mm in diameter (the standard threshold for significant lesions) are therefore visible in only one image. Thus, it is impossible to create a 3D model of a smaller tumour using only MR images of transversal slices. For tumours of medium size, the number of contributing slices is usually three, but in some cases it may be up to four or five. Sequences of three segmented MR slices are considered as input data for the reconstruction approach, as it is the most frequent situation. However, our approach can be easily adapted for longer input sequences. In any input cross-section, the interior of the tumour does not contain any holes and is represented by a single compact region. The following sub-sections present the main steps of the reconstruction process.

2.1 Shape alignment

A morphing process is impossible between two planar (xy) shapes that do not overlap, when viewed in the z -direction, thus in the general case shape alignment is necessary prior to morphing. In the particular case of liver tumours, their nodular appearance always results in a partial overlap between adjacent slices. Thus, shape alignment is not absolutely necessary for liver tumours, but plays nevertheless an important role in the design of our reconstruction approach because the morphing process obtains best results when the common area shared by the two input shapes is maximal. To align two shapes we use a simple translation-based method. Only one shape is translated, while the other one remains immobile and is considered as reference. The search of maximal overlap may result in more than one possible translation. In order to provide a unique solution, we minimize the Hausdorff's distance between the contours of the translated and the reference shape.

Figure 2 presents the results of shape alignment for two configurations of the input data. Two displacements are computed, t_1 and t_3 for objects $obj1$ and $obj3$ respectively, considering $obj2$ as a reference object.

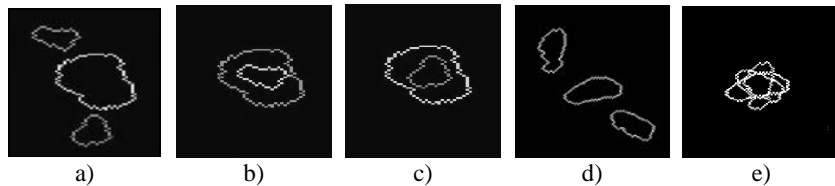


Figure 2. a) An example of input configuration, containing the initial relative position of $obj1$ (top), $obj2$ (middle) and $obj3$ (bottom) ; b) alignment of $obj1$ with respect to $obj2$; c) alignment of $obj3$ with respect to $obj2$; d) another example of input configuration, containing $obj1$, $obj2$ and $obj3$; e) shape alignment of $obj1$ and $obj3$ with respect to $obj2$.

The aligned sequence of binary objects $obj1t$, $obj2$ and $obj3t$ represents the input data for the next step, that is the morphological morphing.

2.2 Morphological morphing based on conditional dilation

We propose a new morphing technique based on conditional dilation.

Definition : Let A and B be two sets, such that $B \subset A$. The conditional dilation of set B using the structuring element K with respect to the reference set A is expressed as :

$$B \oplus K|_A = \left(\bigcup \{B_k | k \in K\} \right) \cap A \quad (1)$$

The input data for this morphing technique consists in an initial binary object $objA$ and a final binary object $objB$, located in adjacent slices. The only constraint imposed to the input configuration is $objA \cap objB \neq \emptyset$, which is always satisfied after shape alignment. Let $objint = objA \cap objB$. The result of this morphing technique is a sequence of intermediate binary objects gradually changing their shape from $objA$ towards $objB$. Figure 3a) contains the contours of $objA$ and $objB$ respectively, while figure 3b) highlights the common area of $objA$ and $objB$.



Figure 3. a) the contours of $objA$ and $objB$; b) the common area shared by $objA$ and $objB$.

In order to gradually transform $objA$ into $objB$ we perform two parallel morphing processes based on conditional dilation. These processes transform $objint$ into $objA$ and into $objB$ using k_1 and k_2 iterations respectively. We name $obj_1(i)$ and $obj_2(i)$ the objects generated after i conditional dilations of $objint$ with respect to $objA$ ($i < k_1$) and, $objB$ ($i < k_2$) respectively. The morphing process transforms $objA$ into $objB$ by generating a sequence of intermediate objects $objAB$ as follows :

$$objAB(i) = \begin{cases} obj_1(k_1 - i) \cup obj_2(i) & \text{if } i < k_1 \leq k_2 \text{ or } i < k_2 \leq k_1 \\ obj_2(i) & \text{if } k_1 \leq i \leq k_2 \\ obj_1(k_1 - i) \cup obj_2(k_2) & \text{if } k_2 \leq i \leq k_1 \end{cases} \quad (2)$$

$i = 1..max(k_1, k_2)$.

The length of the morphing sequence is equal to the largest number among k_1 and k_2 . For input data containing three parallel equidistant tumour slices, two morphing sequences are to be integrated in the 3D tumour model : the sequence obj_{12} of length L_{12} , which gradually transforms obj_1 into obj_2 and the sequence obj_{23} of length L_{23} which gradually transforms obj_2 into obj_3 . The intermediate objects in the morphing sequences are to be located in equidistant planes. Since the lengths L_{12} and L_{23} are usually different, we eliminate $|L_{13} - L_{23}|$ intermediate objects from the longer sequence.

Due to the anisotropy of the conditional dilation, it is possible to encounter very slow shape variations between adjacent intermediate objects at some instances of the morphing process. In order to achieve a quasi-uniform rate of shape change in the sequence of intermediate shapes, we eliminate “redundant” intermediate objects by using a *distance measure*, defined as $d(obj_1, obj_2) = \text{card}(obj_1 \Delta obj_2)$ where obj_1 , obj_2 are adjacent objects in the morphing sequence and Δ stands for the symmetric difference. At iteration k , a *redundancy coefficient* is assigned to every intermediate object of the input sequence :

$$R(obj(i)) = \min\left(\text{dist}(obj(i), obj(i-1))^{-1}, \text{dist}(obj(i), obj(i+1))^{-1}\right) \quad (3)$$

$i = 1..L(k)$, where $L(k)$ is the length of the input sequence at iteration k .

The first and the last objects of the input sequence cannot be eliminated, since they represent input slices in the reconstruction process. The object with the highest redundancy coefficient is eliminated at the current iteration, and the resulting sequence represents the input for the next iteration. The redundancy coefficients are updated at each iteration.

The equal-length constraint for the two morphing sequences results in a uniform inter-slice resolution of the 3D reconstructed model. Furthermore, we use the method of redundancy coefficients for varying the common length of the morphing sequences. Both equal-length sequences can be shortened by eliminating a given number of intermediate objects. Thus, we are able to generate 3D tumour models of variable size and adjustable inter-slice resolution.

Once the two morphing sequences are adjusted to the same length, the 3D interpolated tumour model is obtained by a simple concatenation of the two sequences. Furthermore, to obtain a tumour model consistent with the input data, we have to reverse the shape alignment process. Since translation is reversible, we replace $obj1t$ and $obj3t$ at their initial locations. The objects belonging to the morphing sequences are also translated, in order to perform a smooth transition from obj_1 to obj_2 and from obj_2 to obj_3 respectively.

2.3 Surface closing

Due to the finite inter-slice distance, the acquisition process does not offer any information about the tumour’s extremities. However, we cannot accept flat-endings in the 3D reconstructed model. To close the surface, we perform a shape-based extrapolation which respects the surface smoothness constraint. We assume that the first and the last horizontal cross-sections of the real tumour are one pixel-sized objects, which is a reasonable assumption for liver tumours.

We create two sequences of closing objects located in horizontal slices. These sequences gradually shrink obj_1 and obj_3 towards pixel P_1 and P_3 respectively. When viewed in the z -direction, pixels P_1 and P_3 are located inside obj_1 and obj_3 respectively, as shown in Figure 4. The length of a closing sequence is set to $(N/2)$, where N is the even-valued length of the morphing sequences.



Figure 4. Pixel $P_1 \bullet$ is located inside obj_1 (top), while pixel $P_3 \bullet$ is located inside obj_3 (bottom)

To obtain smooth closing, pixels P_1 and P_3 are chosen to be the centroids of obj_1 and obj_3 respectively. This choice is justified by the fact that real liver tumours are egg-shaped. The centroid of an object is defined as the pixel inside the object which generates this object in a minimum number of conditional dilations.

To generate a closing sequence from an initial 2D object and its centroid, the distances from the centroid to each pixel in the object's boundary are computed. We use a parametric representation for the contour of the object, which allows the storage of the contour pixels in a 1D array. Therefore, the distances from the centroid to the contour pixels are as follows :

$$DIST(k) = \sqrt{(x - X(k))^2 + (y - Y(k))^2} \quad K = 1..length(X) \quad (4)$$

where (x, y) are the coordinates of the centroid and $X(k), Y(k)$ are the coordinates of the k^{th} element in the contour parametrisation. These distances are to decrease gradually towards 0 in $N/2$ iterations, where N is the length of the morphing sequences. More explicitly, we generate $N/2$ intermediate closing contours which shrink gradually towards the centroid. Choosing a linear decreasing pattern leads to an angular, disturbing appearance of the closing parts of the object. Instead, we set the difference between the distances computed at two successive iterations to be proportional to the index of the last iteration :

$$DIST(k)_i - DIST(k)_{i-1} = i \quad (\forall) k = 1..length(X) \quad (5)$$

where i is the index of the iteration, $i = 1..L/2$.

Next, the closing sequences are concatenated at the corresponding extremities of the interpolated 3D tumour model. Furthermore, a surface rendering technique is used to generate a triangular mesh on the external surface of the reconstructed tumour model.

2.4 Surface fairing

The previously described morphological morphing and surface closing processes should result in a 3D object with a smooth surface. However, local irregularities may occur. Some possible reasons for their presence are : a) the shape of the elementary structuring element in the 2D discrete space used in conditional dilation; b) the constraint of integer horizontal displacements in the translation of intermediate cross-sections; c) the successive elimination of intermediate objects with high-valued redundancy coefficients; d) the fixed length of the closing sequences.

We consider Taubin's surface fairing algorithm [7] for its linear complexity and for the fact that it moves the vertices of the mesh without changing the connectivity of the

faces. The fairing process conserves the number of vertices and faces, thus allowing us to compare and measure the smoothness of the faired surface and of the original surface.

3. Reconstruction results and geometric evaluation

The geometric validation of the 3D liver tumour model does not compare this model to the real tumour, since there is a big gap between the amount of input information (3 serial tumour cross-sections) and the amount of output data ($2L+1$ object cross-sections, $L \geq 6$). As a consequence of undersampling, no technique can guarantee to reconstruct the actual anatomy from any set of cross-sections. However, since it contains the three input cross-sections at the original z-levels as specified in the acquisition process, the model is coherent with the input data. Taubin's surface fairing algorithm [5] smoothes the shape of the 2D cross-sections corresponding to the input data, but it performs no shrinking or expanding.

Since the proposed 3D reconstruction approach aims towards a smooth transition between adjacent input shapes and towards a smooth 3D surface closing, we propose a measure of surface smoothness for result evaluation. For each vertex P, the normals to every triangular face containing P are computed, using the classical parametric equations.

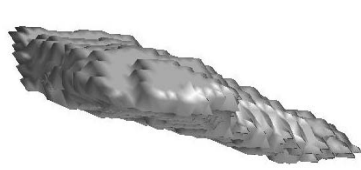
Among the k normals corresponding to P we arbitrarily choose a reference direction (l_0, m_0, n_0) , and compute the cosine of the angle between every normal in the set and the reference direction. The average value $\overline{\cos \alpha / P}$ of $\cos \alpha_i$, $i = \overline{1, k-1}$ represents a local measure of smoothness at vertex P. The local smoothness at P increases when $\overline{\cos \alpha / P}$ approaches 1. A global smoothness measure is represented by the histogram of local smoothness measures computed over the entire surface. The histogram of a smooth surface presents a peak value near 1, and low values elsewhere.

The input sequence in Figure 5a) was interpolated using morphing based on conditional dilation. Shape-based extrapolation for surface closing was performed afterwards. The surface fairing process consisted in two iterations of Taubin's algorithm [5]. The results and evaluation of the reconstructed 3D model are shown in Figure 5.

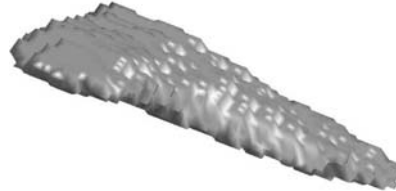
The reconstructed 3D tumour model presented in Figure 5 shows a reasonable quality of surface smoothness even before the fairing process. However, the surface fairing considerably improves the surface smoothness without changing the global appearance of the object.



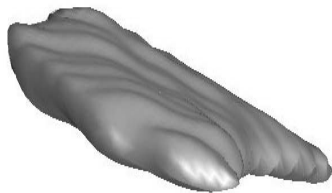
a) input configuration, viewed in the z-direction



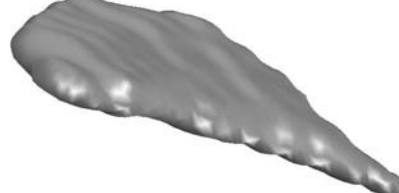
b) $N=6$, before smoothing



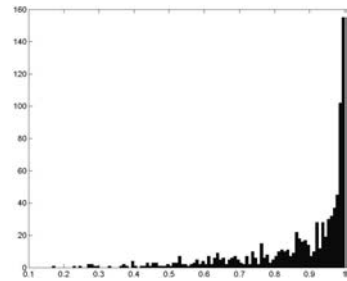
c) $N=6$, before smoothing (different view)



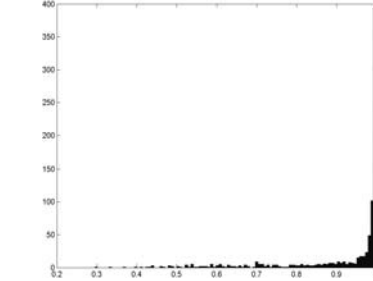
d) $N=6$, after smoothing, same view as in a)



e) $N=6$, after smoothing, same view as in b)



f) smoothness histogram before smoothing



g) smoothness histogram after smoothing

Figure 5. Results and evaluation for the reconstruction approach using morphing based on conditional dilation and shape-based extrapolation; N is the length of the morphing sequence.

4 Mechanical model

Reconstructed 3D tumour models are to be integrated into a complete system for the simulation of cryosurgery of liver cancer. A mechanical model has been developed for this simulator and was presented in [8]. In this section we present the integration of

this mechanical model with a 3D tumour model reconstructed by the algorithm described in section 2.

Our mechanical model uses on the finite element based tensor-mass algorithm [9], which computes forces from a combination of local stiffness tensors attached to every mesh element. These tensors depend only on the mesh geometry at rest, and on the mechanical properties of the tissue. Therefore they can be computed in a preliminary step, while computation in the actual simulation is limited to a linear combination of stiffness matrices and displacement vectors, meeting real-time constraints.

We have previously shown that it is possible to extend the linear tensor-mass model in order to simulate different types of non-linear and visco-elastic mechanical properties [8][10]. Previous results were obtained using meshes consisting of a regular assembly of cubic elements divided into tetrahedrons. We show in this section that the same mechanical model can be applied on a non-uniform mesh derived from an reconstructed 3D tumour model. The mechanical tissue properties used for testing were obtained from experimental *in vitro* compression on deer liver membrane by a biopsy needle [8], since no *in vivo* mechanical data of liver tumour could be measured so far.

The faired triangular surface mesh obtained in section 3 was first transformed into a tetrahedral volume mesh using the Geopack package [11]. Next, compression of this mesh was simulated using the mechanical parameters measured experimentally. Figure 6a) presents five independent experimental force measurements, as well as the simulated force on the reference mesh used to fit our model parameters, and the simulated force computed on the non-uniform tumour mesh.

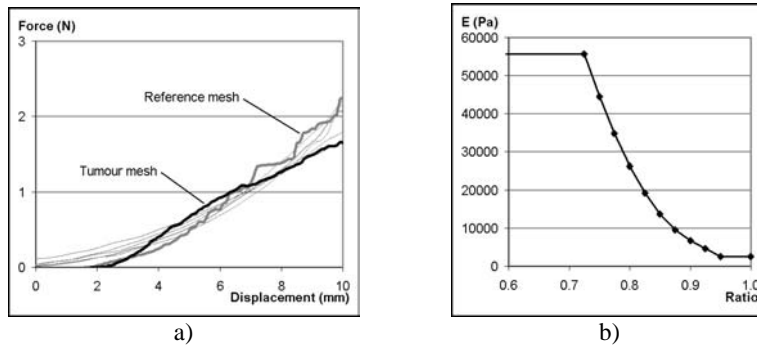


Figure 6. a) Five independent experimental measurements of forces in compression of a deer liver sample by a biopsy needle (light grey curves), and simulated forces computed by a non-linear tensor-mass algorithm on the reference mesh and on a reconstructed 3D tumour model. Compression speed was in all cases constant at 10 mm/s. b) Non-linear function introduced into the tensor-mass algorithm to obtain the simulated curves in a). Non-linearity is expressed as a function of a value quantifying local deformation, which is the ratio of the current tetrahedron mean ratio on the tetrahedron mean ratio at rest.

Although differences can be observed between the two simulations due to the different mesh geometries, accordance between experimental data and both simulations can be considered satisfactory. Due to the thin the tumour geometry (approximately 8 mm in thickness), forces on the tumour mesh tend to increase more slowly at higher deforma-

tions, as it becomes almost entirely pierced. This comparison shows that the proposed mechanical model can be successfully applied to variable geometries. The accurate mechanical parameters of liver tumours remain yet to be determined.

The tissue model derived from these measurements was highly non-linear. Figure 6b) shows the non-linear function introduced into the tensor-mass model to account for these properties. For low deformations the Young modulus was $E = 3600$ Pa, and the Poisson coefficient was kept constant at $\nu = 0.4$.

Figure 7 shows a few deformed mesh configurations at different time steps. The tumour mesh contained 1135 vertices and 3535 tetrahedrons, and a computation rate of 50 iterations per second was achieved on a 2 GHz Pentium III computer.

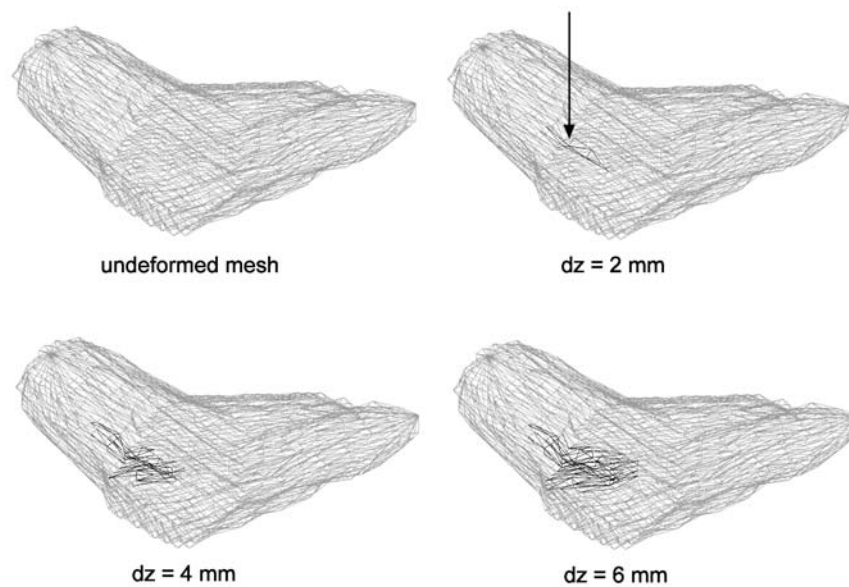


Figure 7. Deformation of a reconstructed 3D mesh under simulated compression by a biopsy needle. The arrow on the second frame shows the position of the needle. Values indicate compression depth, and deformed mesh elements are highlighted.

Conclusion

In this paper, we proposed a new 3D reconstruction technique integrating morphological morphing between adjacent slices and shape-based extrapolation of extremity slices. The presented reconstruction algorithm is appropriate for modelling anatomical structures and was successfully integrated with a biomechanical model allowing fast computation of deformations and force-feedback. However, the accurate mechanical properties of liver tumours *in vivo* remain to be measured. Future work will focus on

the 3D reconstruction of the entire liver and its hepatovascular system from 2D MR cross-sections. Furthermore, tumour and liver geometries are to be integrated with their specific mechanical and thermal models into a complete planning and simulation system for image-guided cryosurgery.

References

1. Goldwasser, S.M., Reynolds, R.A., Talton, D.A., and Walsh, E.S.: Techniques for the rapid display and manipulation of 3-D biomedical data. *Comput. Med. Imag. Graphics*, Vol.12 (1998), 1-24
2. Goshtasby, A., Turner, D.A., and Ackermann, L.V.: Matching of tomographic slices for interpolation. *IEEE Trans. Med. Imag.*, Vol.12 (1993), 366-379
3. Delingette, H. : General Object Reconstruction based on Simplex Meshes. *International Journal of Computer Vision*, Vol.32 (1999), 111-146
4. Herman, G., T., Zheng, J., and Buchholtz, C., A.: Shape-Based Interpolation. *IEEE Computer Graphics and Applicat.*, Vol.12 (1992), 69-79
5. Bors, A., Kechagias, L., and Pitas, I.: Binary morphological shape-based interpolation applied to 3-D tooth reconstruction. *IEEE Trans. Med. Imag.*, Vol.21 (2002), 100-108
6. Branzan-Albu, A., Moisan, C., and Laurendeau, D.: Tumour detection in MR liver images by integrating edge and region information. *Proc. MS4CMS '02 (Modelling and Simulation for Computer-aided Medicine and Surgery, Rocquencourt, France, 12-15 November 2002)*
7. Taubin, G.: A signal processing approach to fair surface design, *Proc. SIGGRAPH'95 (Los Angeles, CA, 6-11 August 1995)*, 351-358
8. Schwartz, J.-M., Dellinger, M., Rancourt, D., Moisan, C., and Laurendeau, D.: Modelling liver tissue properties using a non-linear viscoelastic model for surgery simulation. *Proc. MS4CMS '02 (Modelling and Simulation for Computer-aided Medicine and Surgery, Rocquencourt, France, 12-15 November 2002)*
9. Cotin, S., Delingette, H., and Ayache, N.: A hybrid elastic model for real-time cutting, deformations, and force feedback for surgery training and simulation. *Visual Computer*, Vol. 16 (2000), 437-452
10. Schwartz, J.-M., Langelier, È., Moisan, C., and Laurendeau, D.: Non-linear soft tissue deformations for the simulation of percutaneous surgeries. *Proc. MICCAI 2001 (Medical Image Computing and Computer-Assisted Intervention, Utrecht, The Netherlands, 14-17 October 2001)*, *Lecture Notes on Computer Science*, Vol. 2208 (2001), 1271-72
11. Joe, B.: GEOMPACK - a software package for the generation of meshes using geometric algorithms. *Adv. Eng. Software*, Vol. 13 (1991), 325-331